JSS Focus Issue on Gallium Oxide Based Materials and Devices

Annealing Induced Interfacial Evolution of Titanium/Gold Metallization on Unintentionally Doped β-Ga_2O_3

Ming-Hsun Lee [1] **and Rebecca L. Peterson** [2,z]

[1] *Department of Materials Science and Engineering, University of Michigan, Ann Arbor, Michigan 48109, USA*
[2] *Department of Electrical Engineering and Computer Science, University of Michigan, Ann Arbor, Michigan 48109, USA*

Here, we study the kinetic evolution of the interface between a Ti/Au metal stack and bulk (010) β-Ga_2O_3 substrate under different annealing conditions using scanning / transmission electron microscopy. We observe distinct processes of interfacial reaction and interdiffusion between the metal films and at the metal-semiconductor junction. Upon rapid thermal annealing (RTA), the as-deposited Ti readily reacts at the β-Ga_2O_3 interface, driven by redox favorability. After a 1-min 470°C N_2 RTA, the interface exhibits two segregated crystalline layers: a ~5 nm Ti-rich (Ti-TiO_x) layer lattice-matched to the β-Ga_2O_3 substrate and a ~3 nm Ga-rich (TiGa_x) layer. A substitutional mechanism is proposed based on the similarity in ionic radii of Ti^{+3}, Ti^{+4}, and Ga^{+3}. After 15-min RTA, the Ga-rich layer is diluted within the Ti-Au matrix, while the Ti-TiO_x layer does not significantly change, and there is no further observable Ga out-diffusion from the substrate. Thus, we propose that the Ti-TiO_x layer acts as a diffusion barrier, even when it is no longer lattice-matched with β-Ga_2O_3. In addition, Ti-rich nanocrystals form within the Ti-Au layer, presumably via the proceeding reactions. The observations here provide insights for contact stack evolution during operation of power electronic devices at elevated temperature.

 [DOI: 10.1149/2.0321907jss]

Manuscript received March 5, 2019. Published March 26, 2019. *This paper is part of the JSS Focus Issue on Gallium Oxide Based Materials and Devices.*

Compound semiconductors (CSs) possess a number of advantageous traits over conventional silicon due to elemental alloying, which induces variations in lattice parameters and optical/ electrical properties. III-V CSs, such as GaAs and InP based materials, enable high speed computing devices and circuits owing to their high electron mobility.[1,2] GaN based materials demonstrate a direct wide bandgap (WBG) enabling applications in light emitting diodes, optoelectronics, as well as high-power and high-frequency devices.[3,4] Oxide semiconductors, with advantages in stability as well as transparent properties, have been tremendously developed in the past few decades.[5] Monoclinic β-Ga_2O_3, among other oxide semiconductors, possesses an ultra WBG, ranging from 4.6–4.9 eV, and has demonstrated enormous potential in next generation power electronics for high-power switching and in deep-UV photodetector applications.[6,7] With its ultra-wide band-gap, Baliga's figure of merit (BFOM) is predicted to be over 34,000 MW cm^{-2}, outperforming that of 4H-SiC and GaN.[6,8–10] Moreover, β-Ga_2O_3 is commercially available in high quality substrates grown using low-cost melting-based techniques.[11–13] Accessibility of controlled n-type doping over a wide range (10^{16}–10^{19} cm^{-3}) with Si, Sn, and Ge provides advantages in device processing, which has enabled compelling research demonstrations of metal-oxide-semiconductor field effect transistors (MOSFETs) and Schottky barrier diodes (SBDs).[14–16]

To exploit the full potential of β-Ga_2O_3 devices, formation of high-quality electrical contacts is a critical issue to address. Excess resistance from electrical contacts must be minimized across ohmic metal-semiconductor junctions.[17] Approaches to realize good ohmic junctions include introducing a heavily doped layer at the surface, proper metal work function selection, and manipulating surface states during process, and all of these techniques have been reported in β-Ga_2O_3 device fabrication.[6,18–20] Until today, nearly all of the devices fabricated use Ti-based metal stacks for contact metallization. However, the stability of junction interface is a detrimental issue which will lead to device failure and Ti-based metallization may not provide a stable contact structure.[20,21] Therefore, at this stage, the mechanism(s) enabling decent ohmic conduction across the inherently unstable Ti/β-Ga_2O_3 interface remains elusive.

To probe the interfacial reactions and to understand the fundamental metal stack evolution under elevated annealing process, we employ scanning / transmission electron microscopy (S/TEM) to study the interface morphology. In this study, the elemental distribution driven by redox reactions is observed, and interfacial crystallographic information is recorded. Furthermore, a kinetic mechanism leading to distinct stages of reactions during annealing is proposed. It is shown that the reaction proceeds leading to morphological changes at the micro- and nano-scale that are likely to influence the transport properties of carriers. The findings and mechanisms discovered here provide insights to guide future identification of alternate contact materials.

Experimental

The 10 × 15 mm^2 (010) unintentionally doped (UID) beta-phase Ga_2O_3 substrates used, grown via edge-define film growth method, were purchased from Tamura Corporation, Japan. The carrier concentration (N_D-N_A) is characterized by capacitance-voltage technique to be 1.4 × 10^{17} cm^{-3}. The sample was first subjected to solvent cleaning with acetone, isopropanol alcohol, and methanol, then blown dry with N_2. Titanium/gold metallization of 50 nm and 1 μm, respectively, are deposited via E-beam evaporation with controlled chamber pressure within the range of 1.1 × 10^{-6} to 3.7 × 10^{-6} torr. Then, the sample was spin-coated with photoresist SPR220 3.0 and diced into 5 mm × 5 mm pieces, followed by solvent cleaning. Three of the pieces then underwent different rapid thermal annealing (RTA) processes with (1) unannealed (as-deposited), (2) 470°C 1-min anneal in N_2, and (3) 470°C 15-min anneal in N_2. TEM samples were then prepared with conventional focus ion beam (FIB) assisted lift-out process. Preparation details of similar electron transparent TEM β-Ga_2O_3 samples were reported in our previous paper.[21] Scanning transmission electron microscopy (STEM) images and energy-dispersive X-ray spectroscopy (EDX) were performed on a JEOL 2100F Analytical Electron Microscope (AEM), and TEM images were taken using JEOL 2010F AEM.

Results and Discussion

Figure 1 shows both high-angle annular dark field (HAADF) images and complementary bright-field (BF) images of the three stages

[z] E-mail: blpeters@umich.edu

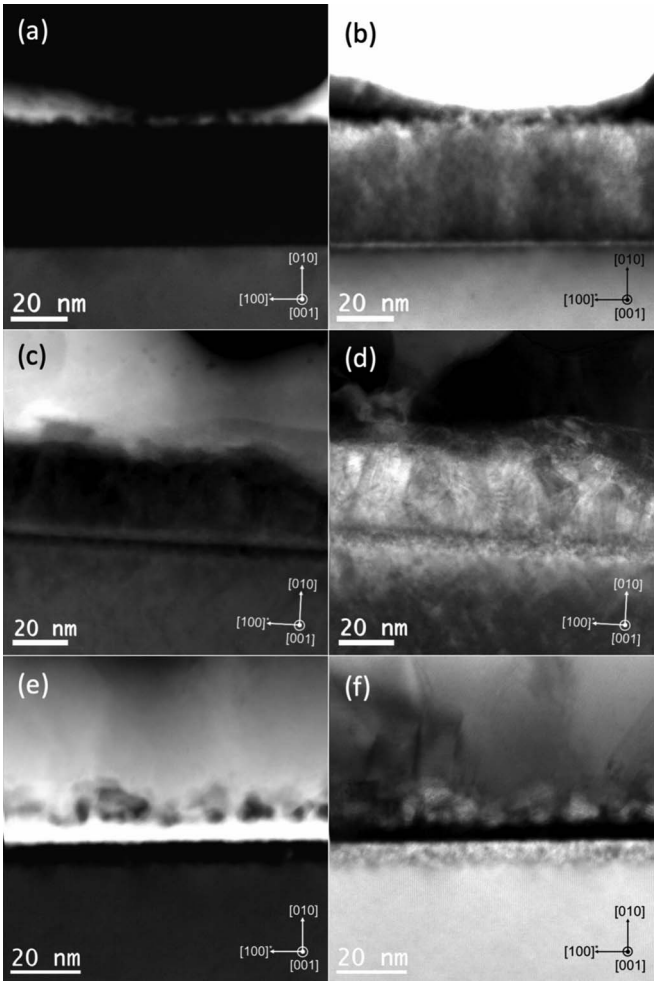

Figure 1. STEM images of the Au/Ti/ β-Ga_2O_3 interface (a-b) as-deposited, (c-d) after 1-min 470°C anneal, and (e-f) after 15-min 470°C anneal. The images in the left column (a, c, and e) are HAADF images while the images in right column (b, d, and f) are complementary BF images.

of evolution of the Au/Ti/ β-Ga_2O_3 structure. With high-angle scattering cross-section scaling with atomic number according to $\sim Z^{1.7}$, the HAADF image mode is often referred to as "Z-contrast" imaging.[22] It thus provides elemental insight in the images. It is observed that, for the 1-min anneal, elemental segregation creates two additional layers at the interface. After EDX analysis, shown in Figure 2b, the two extra layers are confirmed to be a Ga-rich layer on top of a Ti-TiO_x layer. Furthermore, based on high resolution TEM (HRTEM) images in Figures 4c and 4d, these two segregated layers exhibit crystalline structures, where the Ti-TiO_x layer is partially lattice matched to the monoclinic β-Ga_2O_3 substrate while the Ga-rich layer appears to be polycrystalline, and likely is a metal alloy, i.e. $TiGa_x$. In addition, a thin layer of defective Ga_2O_3 right below the Ti/ Ga_2O_3 interface is observed, as previously reported by Higashiwaki et al.[18]

After a prolonged annealing process (15 minutes), the Ti/Au metallization no longer preserves a clear interface but rather is intermixed. Similar to what we observed previously in our study of 1 min 470°C anneal at Ti (20 nm)/Au (50 nm) on Sn-doped β-Ga_2O_3,[21] Ti-rich nanocrystals with diameter around 5 nm form, embedded in an Ti-Au intermixed matrix located around 4 nm above the Ti/Ga_2O_3 interface. These nanocrystals are shown in Figures 4e and 4f. The ~5 nm Ti-TiO_x layer, adjacent to the Ti-Au intermixed matrix, does not significantly grow during the prolonged anneal. Also, there is no further Ti and Ga exchange observed which suggests that the Ti-TiO_x layer formed in situ acts as a diffusion barrier at the interface. Although spatially the Ti-TiO_x layer is localized at the interface, structurally after the prolonged anneal it is no longer latticed-matched to the substrate, as shown in Figures 4e and 4f. Nonetheless, a shallow layer of defective Ga_2O_3 is still observed. It is suspected that the Ti-rich nanocrystals are the products of the proceeding reaction while, due to the thick metal film, the nanocrystals are not readily observed until after the 15-min anneal.

The overall interfacial reaction between Ti/Ga_2O_3 can be understood as redox reactions whose favorability in forming TiO_x at the metal-semiconductor surface has been reported in previous studies.[20,21] The readily-reacted interface of the as-deposited condition is observed here (shown in Figures 1a, 1b, 4a, and 4b), which accounts for the ongoing reaction at room temperature. Ramping up the substrate temperature to the annealing condition of 470°C, an ohmic annealing temperature that is widely reported and used,[18] increases the difference in Gibb's free energy, implying the acceleration of reaction kinetics. The transient interfacial states of the 1-min anneal compared with the excess 15-min anneal provides evidence for the proceeding reaction.

The mechanism of the above-mentioned observations of different stages is proposed to be a sequence of interdiffusion as well as interfacial reactions. These are shown schematically in Figure 3. During the first minute of the anneal, Ti diffuses downward, where it reacts and steals oxygen from Ga_2O_3 by substituting Ga atoms in the substrate. These substituted Ga atoms react with Ti to form a thin localized Ga-rich layer, likely to be $TiGa_x$, sitting on top of Ti-TiO_x layer (the Ti-rich layer shown in Figure 2b). Given the fact that the ionic radii[23] of Ga^{+3}, Ti^{+4}, and Ti^{+3} are 62 pm, 61 pm, and 67 pm, respectively, substitution and inter-diffusion are to be expected, especially at elevated temperature. Upon annealing for longer periods, beyond the first minute, Ti and Au continue interdiffusion. Au diffuses downward and Ti becomes diluted in the Au matrix, forming a Ti-Au intermixed layer. In addition, the localized Ga-rich layer (possibly $TiGa_x$) also becomes diluted in the Ti-Au intermixed matrix, which accounts for the disappearance of the Ga-rich layer in the 15-min microscopy images. Furthermore, during the prolonged anneal, the localized Ti-TiO_x layer did not grow in a significant fashion suggesting that this layer effectively serves as a diffusion barrier preventing further interdiffusion and substitution between Ti and Ga. The observed Ti-rich nanocrystals (likely to be TiO_x) embedded in the Ti-Au intermixed layer are likely to be products of the proceeding reactions. Although the reason that the Ti-rich nanocrystals are located ~5 nm above the Ti-TiOx region is not clear, it may be that further growth and aggregation of these nanocrystals may form a layer that acts as a barrier for carrier transport. Thus the electrical properties of the interface may degrade upon prolonged anneals. Alternately, these nanocrystals may play a negligible role in vertical conduction, due to the surrounding metal alloy (Ti-Au-Ga) matrix, in which case the electrical properties of the interface may be stable.

These observations are consistent with our previous findings on Ti/Au ohmic contacts to Sn-doped Ga_2O_3, which used a 1-min 470°C RTA process.[21] First, the lattice-matching feature in Ti-rich layer (likely to be TiO_x) is observed in both studies for the 1-min anneal case. Second, the defective Ga_2O_3 layer is seen after 1-min annealing in both studies. However, the Ti-rich nanocrystals embedded in the Ti-Au intermixed metallic film are observed only in the prolonged-anneal condition tested in this study. In this study, we used 50-nm Ti and 1 μm Au on UID Ga_2O_3, whereas a similar feature is seen after a 1-min anneal in the previous study, which used a 20-nm Ti and 80-nm Au on degenerately Sn-doped Ga_2O_3. This comparison suggests that: (a) substrate dopant and doping level does not play a primary role in determining the interfacial reactions and interdiffusion between Au/Ti/ Ga_2O_3; and (b) the difference in Ti film thickness may play a more important role in influencing the kinetics of diffusion and reaction at the interface. These conclusions are corroborated by microscopy of 20-nm Ti and 80-nm Au on UID Ga_2O_3 annealed for one minute, shown in Supplemental Information. With a thicker Ti/Au layer, the overall reaction is retarded and transient states were recorded. The Ti-TiO_x and Ga-rich layers formed during the 1-min

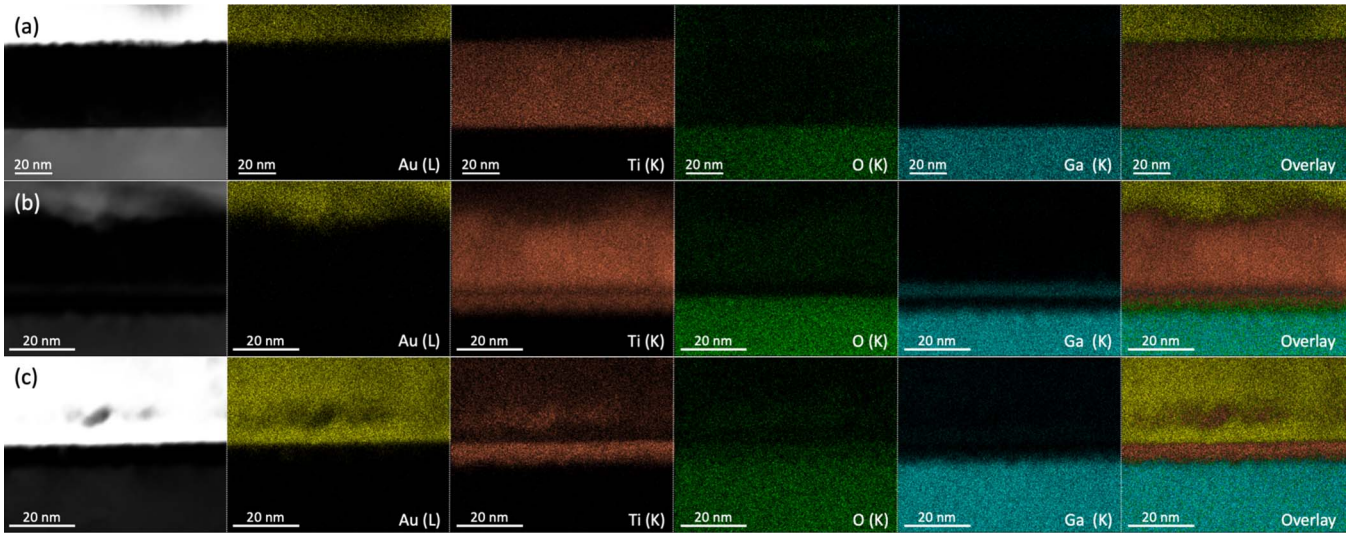

Figure 2. EDX mapping of the Au/Ti/ β-Ga_2O_3 interface at different stages in the annealing process: (a) as-deposited; (b) after a 470°C 1-min N_2 anneal; and (c) after a 470°C 15-min N_2 anneal. The elemental distribution counts are shown: yellow, orange, green, and blue represent Au (L), Ti (K), O (K), and Ga (K), respectively. Note the distinct Ti-TiO_x and Ga-rich layers in (b). Also note that in (c), Ti-rich nanocrystals are observed and the Ti-TiO_x layer remains roughly the same thickness as in (b).

annealing condition in the current UID study appear to be a transient state. Moreover, the observed lattice matching of the Ti-TiO_x layer with the substrate also appears to be a transient feature that was not observed in the over-annealed condition. Based on this, it is hypothesized that the lattice matched Ti-TiO_x provides a relatively low barrier to electron transport. However, after the prolonged anneal, changes in the crystallographic structure may change the electrical behavior of the junction. Further studies are needed to correlate the microstructure observed under prolonged anneals with electrical behavior of the metal-semiconductor contact. In addition, in the future it may be interesting to investigate the role of additional metallization layers such as Ti/Al/Ni/Au on Ga_2O_3, which has been used in other works.[24,25]

Conclusions

The kinetic evolution of the Au/Ti/ β-Ga_2O_3 interface is observed here with a relatively thick metallic Ti (50 nm)/Au (1 μm) layer. The Ti/ β-Ga_2O_3 interface shows readily reacted features in the as-deposited condition. After a 1-min anneal, the interface shows a segregated Ga-rich layer on top of a Ti-TiO_x layer. The Ti-TiO_x, at this stage, is partially lattice matched with the β-Ga_2O_3 substrate. After a prolonged anneal of 15-min, we observe numerous Ti-rich nanocrystals embedded in a Ti-Au intermixed matrix, adjacent to the Ti-TiO_x layer. The spatially localized Ti-TiO_x layer, however, does not preserve the lattice-matching feature after the prolonged anneal, and there is also no further exchange of Ga and Ti observed. Therefore we conclude that the Ti-TiO_x layer formed in situ serves as an effective diffusion barrier to further Ti/Ga interdiffusion. Also, the Ti-rich nanocrystals are likely to be products of proceeding reactions. The partially lattice-matched Ti-TiO_x is shown to be a transient feature and likely provides a low barrier to carrier transport across the interface. The micro- and nano-structural changes resulting from the aforementioned reactions have been imaged in this study. Based on these results, further work is needed to correlate the interfacial changes with electrical properties of the interface. Due to the formation of the Ti-TiO_x layer and the Ti-rich nanocrystals, the interface may or may not be electrically stable.

Acknowledgments

This work was supported by the Department of the Navy, Office of Naval Research under ONR Award No. N00014-17-1-2998 with Dr. Paul Maki. Any opinions, findings, and conclusions or recommendations expressed in this material are those of the author(s) and do not necessarily reflect the views of the Office of Naval Research. Portions of this work were conducted in Lurie Nanofabrication Facility (LNF) and Michigan Center for Materials Characterization $(MC)^2$, which are supported by the University of Michigan College of Engineering. The FEI Nova 200 Nanolab, JEOL 2010F AEM and JEOL 2100F AEM instruments were funded by NSF Award Nos. DMR-0320740, DMR-9871177, and DMR-0723032, respectively.

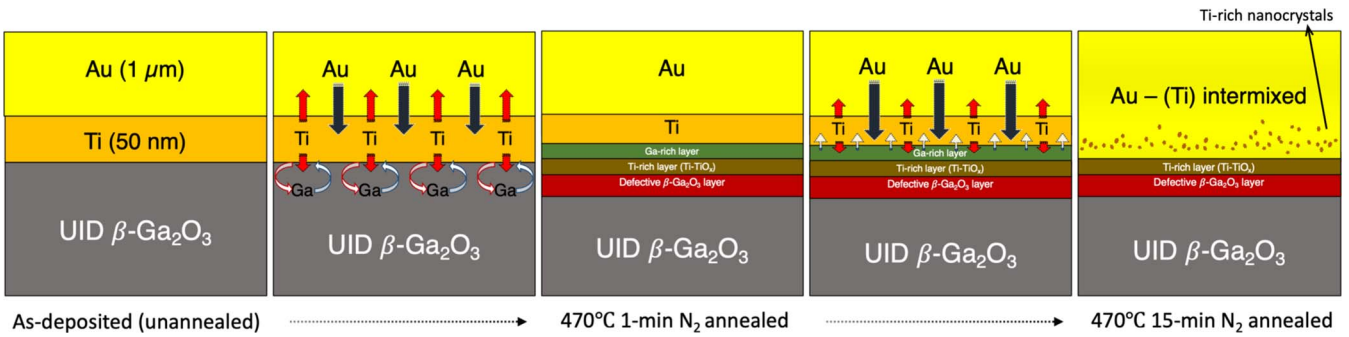

Figure 3. A schematic of the proposed evolution of the Au/Ti/ β-Ga_2O_3 interface during 470°C annealing.

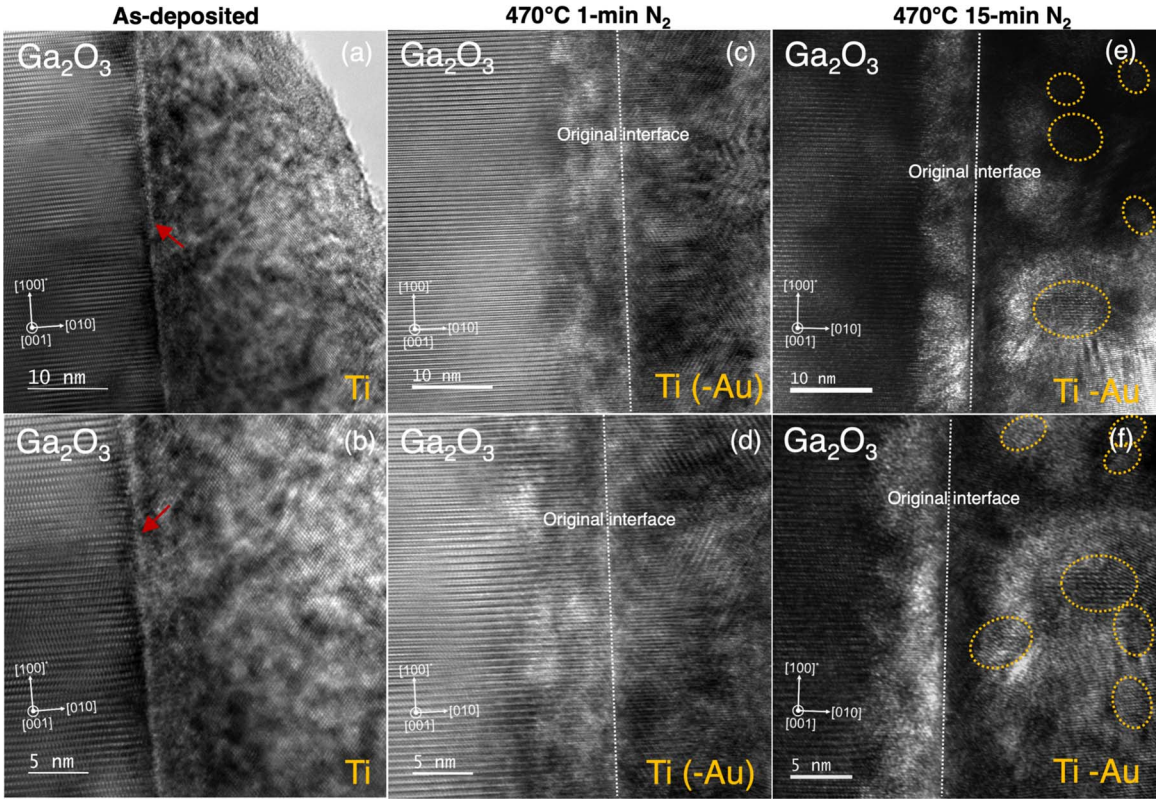

Figure 4. HRTEM images of the interfacial structures at three different stages: (a-b) as-deposited; (c-d) after a 470°C 1-min anneal; and (e-f) after a 470°C 15-min anneal. Arrows in (a) & (b) indicate the reacted interface, which induced a distorted lattice arrangement of β-Ga_2O_3 near the interface. In (c) & (d), the Ti-TiO_x region just above the original Ti/Ga_2O_3 interface shows partial lattice-matching to the bulk Ga_2O_3. In (e) & (f), the dotted-line circles indicate the observed Ti-rich nanocrystals.

ORCID

Ming-Hsun Lee https://orcid.org/0000-0001-7693-2187
Rebecca L. Peterson http://orcid.org/0000-0001-9405-6539

References

1. J. S. Blakemore, *J. Appl. Phys.*, **53**, R123 (1982).
2. X. Duan, Y. Huang, Y. Cui, J. Wang, and C. M. Lieber, *Nature*, **409**, 66 (2001).
3. R. Quay, *Gallium Nitride Electronics*, p. 470, Springer-Verlag Berlin Heidelberg, (2008).
4. B. J. Baliga, *Semicond. Sci. Technol.*, **28**, 074011 (2013).
5. H. Ohta, K. Nomura, H. Hiramatsu, K. Ueda, T. Kamiya, M. Hirano, and H. Hosono, *Solid-State Electron.*, **47**, 2261 (2003).
6. S. J. Pearton, J. Yang, P. H. Cary, F. Ren, J. Kim, M. J. Tadjer, and M. A. Mastro, *Appl. Phys. Rev.*, **5**, 011301 (2018).
7. M. Higashiwaki, K. Sasaki, H. Murakami, Y. Kumagai, A. Koukitu, A. Kuramata, T. Masui, and S. Yamakoshi, *Semicond. Sci. Technol.*, **31**, 034001 (2016).
8. S. Fujita, *Jpn. J. Appl. Phys.*, **54**, 030101 (2015).
9. M. Higashiwaki, K. Sasaki, H. Murakami, Y. Kumagai, A. Koukitu, A. Kuramata, T. Masui, and S. Yamakoshi, *Semicond. Sci. Technol.*, **31**, 034001 (2016).
10. T. Onuma, S. Saito, K. Sasaki, T. Masui, T. Yamaguchi, T. Honda, and M. Higashiwaki, *Jpn. J. Appl. Phys.*, **54**, 112601 (2015).
11. Z. Galazka, K. Irmscher, R. Uecker, R. Bertram, M. Pietsch, A. Kwasniewski, M. Naumann, T. Schulz, R. Schewski, D. Klimm, and M. Bickermann, *J. Cryst. Growth*, **404**, 184 (2014).
12. N. Ueda, H. Hosono, R. Waseda, and H. Kawazoe, *Appl. Phys. Lett.*, **70**, 3561 (1997).
13. T. Oishi, Y. Koga, K. Harada, and M. Kasu, *Appl. Phys. Express*, **8**, 031101 (2015).
14. K. Konishi, K. Goto, H. Murakami, Y. Kumagai, A. Kuramata, S. Yamakoshi, and M. Higashiwaki, *Appl. Phys. Lett.*, **110**, 103506 (2017).
15. X. Yan, I. S. Esqueda, J. Ma, J. Tice, and H. Wang, *Appl. Phys. Lett.*, **112**, 032101 (2018).
16. K. Zeng, A. Vaidya, and U. Singisetti, *IEEE Electron Device Lett.*, **39**, 1385 (2018).
17. D. K. Schroder, *Semiconductor Material and Device Characterization*, p. 800, John Wiley & Sons, (2006).
18. M. Higashiwaki, K. Sasaki, A. Kuramata, T. Masui, and S. Yamakoshi, *Appl. Phys. Lett.*, **100**, 013504 (2012).
19. M. J. Tadjer, in *Gallium Oxide: Technology, Devices and Applications*, Eds. S. Pearton, F. Ren, and M. Mastro, *Metal Oxides Series*, Ed. G. Korotcenkov., p. 211, Elsevier (2019).
20. Y. Yao, R. F. Davis, and L. M. Porter, *J. Electron. Mater.*, **46**, 2053 (2017).
21. M.-H. Lee and R. L. Peterson, *APL Mater.*, **7**, 022524 (2019).
22. O. L. Krivanek, M. F. Chisholm, V. Nicolosi, T. J. Pennycook, G. J. Corbin, N. Dellby, M. F. Murfitt, C. S. Own, Z. S. Szilagyi, M. P. Oxley, S. T. Pantelides, and S. J. Pennycook, *Nature*, **464**, 571 (2010).
23. W. M. Haynes, *CRC Handbook of Chemistry and Physics, 96th Edition*, p. 2652, CRC Press, (2015).
24. K. D. Chabak, N. Moser, A. J. Green, D. E. Walker Jr., S. E. Tetlak, E. Heller, A. Crespo, R. Fitch, J. P. McCandless, K. Leedy, M. Baldini, G. Wagner, Z. Galazka, X. Li, and G. Jessen, *Appl. Phys. Lett.*, **109**, 213501 (2016).
25. E. Farzana, E. Ahmadi, J. S. Speck, A. R. Arehart, and S. A. Ringel, *J. Appl. Phys.*, **123**, 161410 (2018).